Spectroscopy of Twisted Bilayer Graphene Correlated Insulators

Dumitru Călugăru, Nicolas Regnault, Myungchul Oh, Kevin P. Nuckolls, Dillon Wong, Ryan L. Lee, Ali Yazdani, Oskar Vafek, and B. Andrei Bernevig

Phys. Rev. Lett. **129**, 117602 — Published 8 September 2022

DOI: 10.1103/PhysRevLett.129.117602

Spectroscopy of Twisted Bilayer Graphene Correlated Insulators

Dumitru Călugăru,[1] Nicolas Regnault,[1] Myungchul Oh,[1] Kevin P. Nuckolls,[1] Dillon Wong,[1] Ryan L. Lee,[1] Ali Yazdani,[1] Oskar Vafek,[2,3] and B. Andrei Bernevig[1,4,5,*]

[1]*Department of Physics, Princeton University, Princeton, New Jersey 08544, USA*
[2]*National High Magnetic Field Laboratory, Tallahassee, Florida, 32310, USA*
[3]*Department of Physics, Florida State University, Tallahassee, Florida 32306, USA*
[4]*Donostia International Physics Center, P. Manuel de Lardizabal 4, 20018 Donostia-San Sebastian, Spain*
[5]*IKERBASQUE, Basque Foundation for Science, Bilbao, Spain*

We analytically compute the scanning tunneling microscopy (STM) signatures of integer-filled correlated ground-states of the magic angle twisted bilayer graphene (TBG) narrow bands. After experimentally validating the strong-coupling approach at ± 4 electrons/moiré unit cell, we consider the spatial features of the STM signal for 14 different many-body correlated states and assess the possibility of Kekulé distortion (KD) emerging at the graphene lattice scale. Remarkably, we find that coupling the two opposite graphene valleys in the intervalley-coherent (IVC) TBG insulators does not always result in KD. As an example, we show that the Kramers IVC state and its nonchiral $\mathrm{U}(4)$ rotations do not exhibit any KD, while the time-reversal-symmetric IVC state does. Our results, obtained over a large range of energies and model parameters, show that the STM signal and Chern number of a state can be used to uniquely determine the nature of the TBG ground-state.

Introduction. Near the first magic angle [1–3], both transport [4–19] and spectroscopy [20–29] experiments have uncovered a wealth of superconducting and correlated insulating phases in twisted bilayer graphene (TBG), sparking considerable theoretical effort towards their understanding [30–74]. The physics of TBG near integer fillings with ν electrons per moiré unit cell was argued to be in the strong coupling regime, dictated by the interaction-only Hamiltonian projected onto its almost-flat bands [43, 44, 59, 64, 69]. The enlarged continuous spin-valley symmetries thereof [43, 44, 59, 75] have rendered a low-energy manifold of its many-body eigenstates [43, 44, 59, 64, 69] and few-particle excitations [64, 76] exactly solvable at integer fillings. Following numerically-validated [56, 59, 70] analytical arguments [43, 59, 69, 75], the resulting eigenstates of the projected interaction Hamiltonian were shown to be energetically-competitive ground-state candidates, if not *the* actual ground states of the system, for a large range of parameters.

Building on the aforementioned theoretical advances, this *Letter* identifies spectroscopic signatures of the various competing states. For a given insulator, the differential conductance measured in scanning tunneling microscopy (STM) experiments is proportional to its spectral function [77], which can be computed analytically from the readily-available many-body electron and hole excitations [64, 76]. We find that the STM features of the proposed correlated states – particularly the presence or absence of a Kekulé distortion (KD) at the graphene lattice scale (*i.e.* the modulation of the STM signal at wavevectors connecting the two graphene valleys) – together with the knowledge of their Chern number, can distinguish among the candidate many-body states. Recent experiments [78–80] demonstrating the ability of STM to visualize symmetry-broken states with KD arising from many-body interactions in the zeroth Landau level of monolayer graphene indicate that similar techniques can be employed to discriminate between the correlated insulators of TBG.

The competing correlated states of TBG at an integer filling ν can be characterized by their Chern number $\mathcal{C}$ and valley polarization, being either valley polarized (VP) or inter-valley coherent (IVC). Additionally, even for $\mathcal{C} = 0$, IVC states may either spontaneously break time-reversal symmetry (T), as in the Kramers IVC (K-IVC) state, or preserve it, as in the T-symmetric IVC (T-IVC) state [43, 44, 59, 75]. Some of these states can be stabilized by magnetic field [12, 15, 17, 26, 27, 81]. In this *Letter*, we analyze numerically 14 different TBG correlated insulators, and show analytically that *all* VP states together with the K-IVC states at $\nu = \pm 2, 0$ exhibit no KD, while generic IVC states do display KD. Furthermore, we show that the strong- versus weak-coupling nature of the system can be uniquely inferred from the spectral function of the $\nu = \pm 4$ band insulator. The correct asymmetric peak structure obtained in the strong-coupling approach differs significantly from the weak-coupling result and shows dramatic variations as the STM tip moves from the AA to AB moiré regions. While the experimental data displays large sample-to-sample variation in the local density of states (LDOS), some data sets are uniquely compatible with strong-coupling description.

Model. The physics of magic-angle TBG is dominated by the repulsive Coulomb interaction Hamiltonian projected in the almost-flat bands near charge neutrality [43, 59, 75, 82]

$$H_I = \frac{1}{2\Omega_{\mathrm{TBG}}} \sum_{\mathbf{q}\in \mathrm{MBZ}} \sum_{\mathbf{G}\in \mathcal{Q}_0} O_{-\mathbf{q}-\mathbf{G}} O_{\mathbf{q}+\mathbf{G}}. \qquad (1)$$

where Ω_{TBG} is the area of the TBG sample, MBZ and

$\mathcal{Q}_0$ respectively denote the moiré Brillouin zone (MBZ) and reciprocal lattice, while

$$O_{\mathbf{q}+\mathbf{G}} = \sum_{\substack{\mathbf{k},\eta,s \\ n,m=\pm 1}} \sqrt{V(\mathbf{q}+\mathbf{G})} M^{\eta}_{mn}(\mathbf{k},\mathbf{q}+\mathbf{G}) \times \left(\hat{c}^{\dagger}_{\mathbf{k}+\mathbf{q},m,\eta,s} \hat{c}_{\mathbf{k},n,\eta,s} - \frac{1}{2}\delta_{\mathbf{q},\mathbf{0}}\delta_{m,n} \right) \quad (2)$$

are proportional to the flat-band-projected density operators. In particular, $\hat{c}^{\dagger}_{\mathbf{k},n,\eta,s}$ is the electron creation operator for the TBG conduction ($n = +1$) and valence ($n = -1$) flat bands from valley $\eta = \pm$ and spin $s = \uparrow, \downarrow$, while $M^{\eta}_{mn}(\mathbf{k},\mathbf{q}+\mathbf{G})$ are the TBG form factors. The Fourier-transformed screened Coulomb potential $V(\mathbf{q}) = 2\pi U_{\xi}\xi^2\left(1-e^{-2\xi q}\right)/(\xi q)$ (with U_{ξ} and ξ respectively denoting the interaction energy scale and the screening length) corresponds to the typical single-gate arrangement of the TBG sample in an STM experiment [26].

The TBG single-particle Hamiltonian features a series of discrete symmetries [82]: the C_{2z}, C_{3z}, T, and C_{2x} *commuting* symmetries, as well as an approximate unitary particle-hole P *anti-commuting* symmetry [75, 83–86]. The latter enlarges the valley-spin-charge $\mathrm{U}(2) \times \mathrm{U}(2)$ rotation symmetry of H_I to the so-called nonchiral-flat $\mathrm{U}(4)$ symmetry [43, 44, 59, 75], henceforth denoted by $\mathrm{U_{nc}}(4)$. Additionally, when the inter-layer tunneling amplitude at the AA stacking centers (w_0) is neglected compared to the one at AB stacking centers ($w_1 = 110\,\mathrm{meV}$) – in the so-called chiral limit ($w_0/w_1 = 0$) – the single-particle Hamiltonian enjoys an additional *anti-commuting* chiral C symmetry [75, 87], which further enlarges the symmetry group of H_I to the chiral-flat $\mathrm{U}(4) \times \mathrm{U}(4)$ group [59, 75]. Recombining the active TBG bands into Chern-number e_Y bands with operators $\hat{d}^{\dagger}_{\mathbf{k},e_Y,\eta,s} = \frac{1}{\sqrt{2}}\left(\hat{c}^{\dagger}_{\mathbf{k},+1,\eta,s} + i e_Y \hat{c}^{\dagger}_{\mathbf{k},-1,\eta,s}\right)$, the 32 generators the chiral-flat $\mathrm{U}(4)\times\mathrm{U}(4)$ group correspond to independent valley-spin rotations within each Chern sector. Away from the chiral limit the $\mathrm{U}(4) \times \mathrm{U}(4)$ generators get combined into the 16 $\mathrm{U_{nc}}(4)$ generators such that $\mathrm{U_{nc}}(4)$ intervalley (intravalley) rotations act on the two Chern sectors in the same (opposite) way [75].

The presence of enlarged symmetries renders some of the eigenstates of H_I exactly solvable at integer fillings. Up to rotations $\hat{U}$ belonging to the symmetry group of H_I, the TBG ground states have been shown to be Slater determinants obtained by populating the active TBG bands one Chern-valley-spin sector $\left(e_{Y_j},\eta_j,s_j\right)$ at a time [43, 56, 59, 69, 70, 75, 76]

$$|\varphi\rangle = \hat{U}\prod_{\mathbf{k}}\prod_{j=1}^{4+\nu}\hat{d}^{\dagger}_{\mathbf{k},e_{Y_j},\eta_j,s_j}|0\rangle\,. \quad (3)$$

In the chiral limit, $|\varphi\rangle$ is an *exact* eigenstate of H_I for any choice of the filled Chern-valley-spin sectors and $\hat{U} \in \mathrm{U}(4) \times \mathrm{U}(4)$ [69]. Away from the chiral limit, only the insulators from Eq. (3) with fully-filled or fully-empty valley-spin flavors and $\hat{U} \in \mathrm{U_{nc}}(4)$ are *exact*, with the rest being *perturbative* eigenstates of H_I [69].

Spectral function. For a given state $|\varphi\rangle$ from Eq. (3), the differential conductance as a function of bias voltage measured in STM experiments is proportional to its spectral function [77]

$$A(\mathbf{r},\omega) = \sum_{\xi,s}\Big[\left|\left\langle\xi\middle|\hat{\psi}^{\dagger}_{s}(\mathbf{r})\middle|\varphi\right\rangle\right|^2\delta(\omega-E_{\xi}+E_{\varphi}) + \left|\left\langle\xi\middle|\hat{\psi}_{s}(\mathbf{r})\middle|\varphi\right\rangle\right|^2\delta(\omega+E_{\xi}-E_{\varphi})\Big]\,. \quad (4)$$

where $\psi_s(\mathbf{r})$ denotes the electron field annihilation operator corresponding to spin $s = \uparrow, \downarrow$, and a summation is performed over all the *many-body* eigenstates $|\xi\rangle$ of H_I with energy E_{ξ} [82]. Expressing the field operators in the TBG energy-band basis $\hat{\psi}^{\dagger}_{s}(\mathbf{r}) = \sum_{\eta,n} V_{\mathbf{r},\mathbf{k}n\eta}\hat{c}^{\dagger}_{\mathbf{k},n,\eta,s}$ (where the factors $V_{\mathbf{r},\mathbf{k}n\eta}$ depend on the carbon p_z orbitals and the TBG flat band wave-functions and include contributions from both graphene layers), we find that

$$A(\mathbf{r},\omega) = \sum_{\substack{\mathbf{k}\in\mathrm{MBZ}, \\ n,\eta,n',\eta' \\ c=\pm}}\left[\mathcal{M}^{c}_{\varphi}(\omega)\right]_{\mathbf{k}n\eta,\mathbf{k}n'\eta'}\left[\mathcal{B}(\mathbf{r})\right]_{\mathbf{k}n\eta,\mathbf{k}n'\eta'}\,. \quad (5)$$

In Eq. (5), we have introduced the spatial factor matrix $[\mathcal{B}(\mathbf{r})]_{\mathbf{k}n\eta,\mathbf{k}'n'\eta'} = V_{\mathbf{r},\mathbf{k}n\eta}V^{*}_{\mathbf{r},\mathbf{k}'n'\eta'}$ (which depends only on the TBG single-particle Hamiltonian) and the spectral function matrices (which depend on the state $|\varphi\rangle$)

$$\left[\mathcal{M}^{c}_{\varphi}(\omega)\right]_{\mathbf{k}n\eta,\mathbf{k}n'\eta'} = \sum_{\lambda_{-c},s}\langle\lambda_+|\hat{c}_{\mathbf{k},n',\eta',s}|\lambda_-\rangle \times\left\langle\lambda_-\middle|\hat{c}^{\dagger}_{\mathbf{k},n,\eta,s}\middle|\lambda_+\right\rangle\delta\left(\omega-E_{\lambda_-}+E_{\lambda_+}\right), \quad (6)$$

where $|\lambda_c\rangle = |\varphi\rangle$ and we assumed no breaking of the moiré translation symmetry. Since a $\hat{c}^{\dagger}_{\mathbf{k},n,\eta,s}$ operator acts in *one* single-layer graphene (SLG) valley, $[\mathcal{B}(\mathbf{r})]_{\mathbf{k}n\eta,\mathbf{k}n'\eta}$ is only modulated at the level of the SLG and TBG lattices. In contrast, $[\mathcal{B}(\mathbf{r})]_{\mathbf{k}n\eta,\mathbf{k}n'(-\eta)}$ contains an additional modulation corresponding to wave-vectors linking the two Dirac points of the same graphene layer, which manifests in real space as a KD of the SLG.

As shown in Eqs. (5) and (6), computing the TBG spectral function requires exact eigenstates of H_I containing an extra electron/hole compared to $|\varphi\rangle$ (*i.e.* the charge-one excitations). Despite H_I being a quartic Hamiltonian, the exact charge-($\pm$)one excitations on top of $|\varphi\rangle$ can be computed as a zero-body problem using the *charge-one commutation relations* [64, 76]. For example, the electron commutation relation reads as

$$\left[H_I-\mu\hat{N},\hat{c}^{\dagger}_{\mathbf{k},n,\eta,s}\right]|\varphi\rangle = \sum_{m}R^{\eta}_{mn}(\mathbf{k})\,\hat{c}^{\dagger}_{\mathbf{k},m,\eta,s}|\varphi\rangle\,, \quad (7)$$

where μ denotes the chemical potential, $\hat{N}$ is the total fermion number operator and the matrix $R(\mathbf{k})$ depends on ν, the active TBG wave-functions and the Coulomb repulsion potential [82]. As such, the $\hat{c}^\dagger_{\mathbf{k},n,\eta,s}$ and $\hat{c}_{\mathbf{k},n,\eta,s}$ operators can be recombined into exact electron and hole excitations, allowing for the analytical calculation of the spectral function of $|\varphi\rangle$ [82].

Signatures of strong correlation. We first analyze the spectral function of the $\nu = -4$ ($\nu = +4$) TBG insulator from Eq. (3), for which the active TBG bands are fully-empty (fully-filled) and no ambiguity in the choice of ground-state arises. As shown in Fig. 1, the strong-coupling and weak-coupling spectral functions at $\nu = \pm 4$ are markedly different as a result of the large interaction-induced dispersion of single-particle excitations in the strong-coupling regime [insets in Figs. 1(b) and 1(e)] compared to the almost-flat dispersion in the weak-coupling (*i.e.* non-interacting) regime, as well as from different van-Hove singularities and Dirac points [64, 76].

We will discuss the $\nu = -4$ insulator from Figs. 1(a)–(c), with the $\nu = +4$ insulator [Figs. 1(d) and 1(e)] following analogously from the many-body charge-conjugation symmetry of TBG [75]. Details about the experimental measurements and signal normalization are provided in Ref. [82]. For $\nu = -4$, we focus on positive-energy biases ($\omega - \mu \geq 0$), such that the electrons tunnel into the fermion states of the active TBG bands, recombined into the electron excitations according to Eq. (7). The electron excitation energies $E^p_{\mathbf{k}}$ [inset of Fig. 1(b)], obtained by diagonalizing the charge-one commutation matrices from Eq. (7) [82], are comprised of four sets of two-fold [spin $\mathrm{SU}(2)$] degenerate bands, which are further paired by the approximate $C_{2z}P$ symmetry of H_I into two sets of almost four-fold degenerate bands [64, 76, 83, 85]. For small bias, the electrons start tunneling into the regions at the bottom of the excitation bands away from any high-symmetry points (*e.g.* halfway between the Γ_M and M_M points of the MBZ), giving rise to the peak near $\omega - \mu \approx 0\,\mathrm{meV}$ in the spectral function at both the AA and AB centers. Upon increasing the bias to $\omega - \mu \approx 20\,\mathrm{meV}$, the electrons tunnel into the almost-flat regions near the boundary of the MBZ, giving rise to two close peaks in the theoretical spectral function, merging into one in the experimental STM signal. For larger biases, the spectral function decreases as the electron tunnel in the strongly-dispersive bands near Γ_M.

The variation of the magnitude of $[\mathcal{B}(\mathbf{r})]_{\mathbf{k}n\eta,\mathbf{k}'n'\eta'}$ with $\mathbf{k} \in$ MBZ at the AA and AB sites [Fig. 1(f)] *qualitatively* explains the change in the STM signal between the two stacking centers: at the AA site, the spatial factor has roughly the same magnitude in the MBZ for the two almost-flat regions of the excitation bands, resulting in similar magnitudes for the LDOS peaks at $\omega - \mu \approx 0\,\mathrm{meV}, 20\,\mathrm{meV}$. At the AB site, the spatial factor has a larger amplitude on the boundary of the MBZ, diminishing the peak at $\omega - \mu \approx 0\,\mathrm{meV}$ compared to the one at $\omega - \mu \approx 20\,\mathrm{meV}$. A similar decrease is also present in the experimental data [Fig. 1(a)], while clearly absent in the non-interacting LDOS [Fig. 1(c)]. Moreover, the half-maximum width of the spectral function ($\Delta\omega$) is much smaller in the non-interacting case ($\Delta\omega < 1\,\mathrm{meV}$, comparable to the active TBG bandwidth) than in the experiment and the strong-coupling prediction ($\Delta\omega = 20 - 30\,\mathrm{meV}$, comparable to $U_\xi = 24\,\mathrm{meV}$ and much larger than the resolution of the experiment $\delta\omega \approx 3\,\mathrm{meV}$ [82]). While the STM signal is sample dependent and may vary from different AA or AB sites, this data set indicates evidence of strong correlations governing the physics of TBG near charge-neutrality.

Discriminating correlated insulating phases. We now investigate the effects of inter-valley coherence on the *spatial* variation of $A(\mathbf{r},\omega)$ for various $|\nu| < 4$ insulating states. Naively, coupling the two graphene valleys in an IVC insulator results in IVC charge-one excitations and should lead to the emergence of KD in the corresponding STM signal. However, due to the discrete symmetries of TBG, breaking the valley $\mathrm{U}(1)$ symmetry does *not* guarantee the emergence of KD in $A(\mathbf{r},\omega)$ [82]. For instance, Figs. 2(a) and 2(b) shows the simulated STM patterns for two *fully* IVC TBG insulators at $\nu = -2$ [59, 69]:

$$
\begin{aligned}
|\text{K-IVC}\rangle &= \prod_{\mathbf{k}} \prod_{e_Y=\pm 1} \frac{\hat{d}^\dagger_{\mathbf{k},e_Y,+,\uparrow} + e_Y \hat{d}^\dagger_{\mathbf{k},e_Y,-,\uparrow}}{\sqrt{2}} |0\rangle\,, \\
|\text{T-IVC}\rangle &= \prod_{\mathbf{k}} \prod_{e_Y=\pm 1} \frac{\hat{d}^\dagger_{\mathbf{k},e_Y,+,\uparrow} + \hat{d}^\dagger_{\mathbf{k},e_Y,-,\uparrow}}{\sqrt{2}} |0\rangle\,.
\end{aligned}
\tag{8}
$$

The K-IVC (T-IVC) state is obtained from a fully-filled valley-spin flavor by rotating the two Chern bands in the xz valley plane in opposite (identical) directions, as shown in Figs. 2(a) and 2(b). Remarkably, while the STM patterns of the T-IVC state show clear signs of KD, no KD emerges for the K-IVC state.

The counter-intuitive absence of KD in the $\nu = -2$ K-IVC state is part of a more general *exact* result, relying on the C_{2z}, T, and P symmetries of TBG [82]: a VP even-ν insulator with only fully-filled and fully-empty valley-spin flavors and all its $\mathrm{U_{nc}}(4)$ rotations have *identical* spectral functions, without exhibiting KD. Note that these are precisely the theoretically-proposed exact ground states of H_I at even filling and away from the chiral limit [43, 59, 69, 70]. Moreover, even when the P symmetry is broken, we find that C_{2z} and T are enough to guarantee the *exact* absence of KD in the K-IVC state, although not necessarily in its general $\mathrm{U_{nc}}(4)$ rotations [82].

When $|\varphi\rangle$ is *not* a $\mathrm{U_{nc}}(4)$ rotation of an insulator with only fully-filled or fully-empty valley-spin flavors, intervalley-coherence *can* lead to KD, but fine-tuned counter-examples do exist. For maximally-spin polarized states, we have derived simple rules governing the presence of KD [82]: 1) Filling a single IVC Chern band gives rise to KD; 2) An exact cancellation of the KD signal

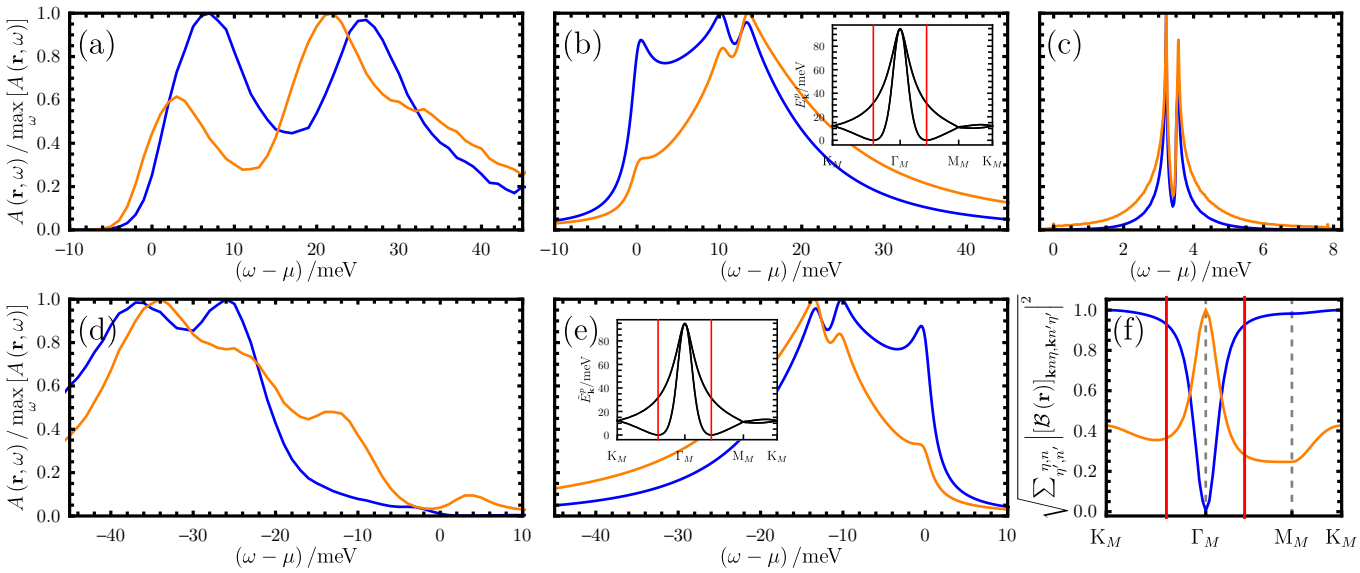

FIG. 1. The TBG spectral function for the $\nu = \pm 4$ insulator. For $\nu = -4$ ($\nu = +4$), we compare the experimentally-measured STM signal in (a) [(d)] with the spectral function computed from the charge-one excitation of H_I in (b) [(e)]. We use $U_\xi = 24\,\mathrm{meV}$, $\xi = 300\,\mathrm{nm}$, $w_0/w_1 = 0.8$. For reference, the TBG spectral function at $\nu = -4$ derived from the single-particle TBG Hamiltonian is given in (c). The signal at the center of the AA (AB) site is shown in blue (orange) and normalized by its maxima in the energy range at that particular location. The theoretically-computed spectral function is averaged over three SLG unit cells. The inset in (b) [(e)] shows the electron [hole] excitation dispersion $E^p_{\mathbf{k}}$ ($\tilde{E}^p_{\mathbf{k}}$) computed from Eq. (7) (the red vertical lines are a guide for eye pointing the minima of the dispersion). (f) provides the spatial factor at the AA and AB sites along the high symmetry line of the MBZ (the red lines indicate the position of minima).

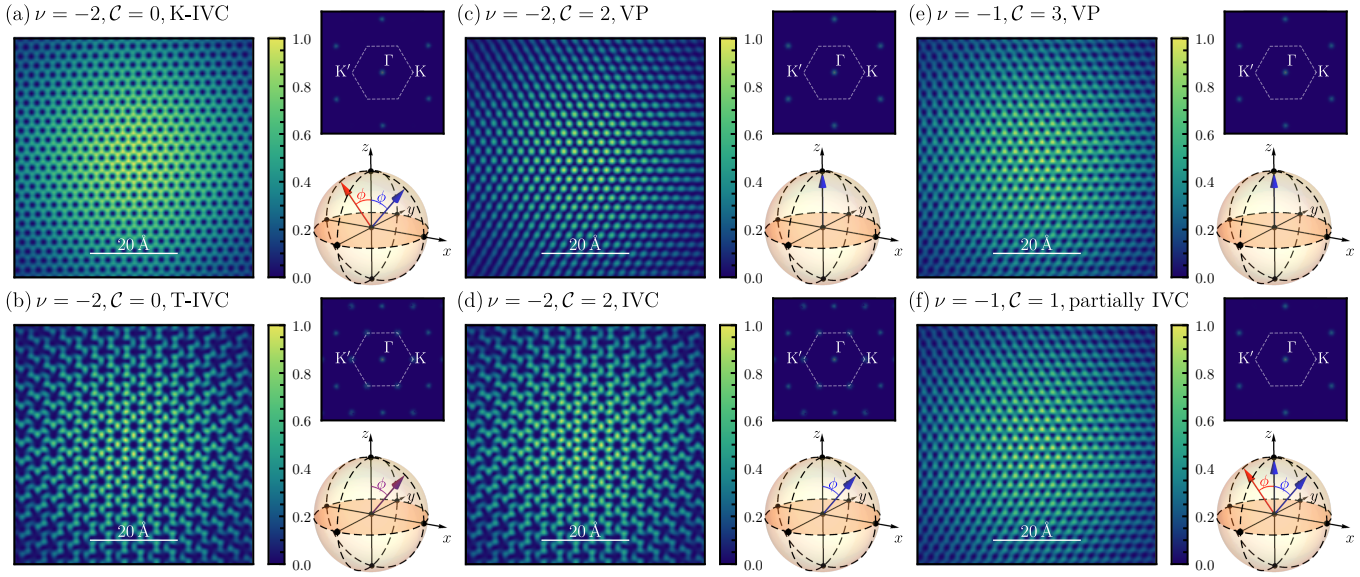

FIG. 2. Kekulé distortion and intervalley-coherence. For each insulator [(a)-(f)], we show the real-space spectral function centered at the AA site (left panel), its Fourier transformation (top-right panel), as well as the valley polarizations of the occupied Chern bands as blue ($e_Y = +1$) or red ($e_Y = -1$) unit vectors in the valley Bloch sphere. The valley polarization can be oriented parallel to the $\hat{\mathbf{z}}$ axis or at an angle $\phi = \pi/2$ to it. We consider the $\nu = -2$, $\mathcal{C} = 0$, K-IVC [(a)] and T-IVC [(b)] states, the $\nu = -2$, $\mathcal{C} = 2$, VP [(c)] and IVC [(d)] Chern insulators, as well as the $\nu = -1$, $\mathcal{C} = 3$ fully VP [(e)] and $\nu = -1$, $\mathcal{C} = 1$ partially IVC [(f)] Chern insulators. The presence of KD in (b) and (d) appears as three-fold enlargement of the SLG unit cell and as a signal at the K and K′ points of the SLG Brillouin zone. We use $U_\xi = 8\,\mathrm{meV}$, $\xi = 300\,\mathrm{nm}$, $w_0/w_1 = 0.8$.

occurs upon filling a pair of Chern bands with *opposite* Chern numbers whose valley polarization projections in the valley xy plane of the Bloch sphere are nonzero and cancel out, *e.g.* the K-IVC from Fig. 2(a). In Figs. 2(c)–

(f), we illustrate these rules for $\mathcal{C} \neq 0$ states, which at odd filling are the theoretical ground-states, while at even filling are the ground-states in-field [12, 15, 17, 26, 27, 81]. The $\nu = -2$, $\mathcal{C} = 2$ and $\nu = -1$, $\mathcal{C} = 3$ VP Chern insulators trivially harbor no KD. The $\nu = -2$, $\mathcal{C} = 2$ IVC insulator does exhibit KD, since the valley polarizations of the two bands projected in the xy plane of the valley Bloch sphere do not cancel out. Finally, the $\nu = -1$, $\mathcal{C} = 1$ partially IVC insulator has one VP filled Chern band and a pair of filled IVC Chern bands, satisfying rule 2 and therefore not displaying any KD. Further examples are presented in Ref. [82]. Between states showing no KD, further LDOS differences exist because the Chern band operators $\hat{d}^{\dagger}_{\mathbf{k},e_Y,\eta,s}$ are primarily located on a single SLG sublattice, depending on $e_Y\eta = \pm 1$. In the $\nu = -2$, $\mathcal{C} = 2$ state, two Chern bands with $e_Y = +1$ are occupied in the same valley $\eta = +$ (and two spin sectors), leading to the appearance of a triangular lattice in the STM signal from Fig. 2(c). To obtain the VP $\nu = -1$, $\mathcal{C} = 3$ (IVC $\nu = -1$, $\mathcal{C} = 1$) state, a Chern band with $\eta = -$, $e_Y = +1$ ($\eta = +$, $e_Y = -1$) is added, which is polarized primarily on the other graphene sublattice. Hence two inter-penetrating triangular lattices of weight 2 : 1 appear in the LDOS patterns from Figs. 2(e) and 2(f).

Conclusions. We analyzed the STM signal of a multitude of the predicted candidates for the correlated insulators in TBG and showed that it can be used to differentiate between the ground-states. Both numerically and analytically, we found that the $\mathcal{C} = 0$ celebrated K-IVC states at $\nu = \pm 2, 0$ do not exhibit a KD, while other IVC states, including the $\nu = \pm 2$ T-IVC or $\mathcal{C} = 2$ states at do display KD. We experimentally measured the STM signal for the $\nu = \pm 4$ band insulator, and used it to validate the the strong-coupling regime. The broadening of the signal and the specific variations of the signal from the AA to the AB sites are unique signatures of the strong-coupling regime. Our work paves the road toward the unambiguous identification of the TBG correlated insulators.

Acknowledgments. We thank Fang Xie for fruitful discussions. During the later stages of preparation of our manuscript, we became aware of Ref. [88] posted on the same date on arXiv, which also computes the STM signal of various TBG states using Hartree-Fock methods. Where they overlap, our conclusions (*i.e.* the vanishing of KD in the K-IVC state) agree with the ones presented in Ref. [88]. The simulations presented in this work were performed using the Princeton Research Computing resources at Princeton University, which is a consortium of groups led by the Princeton Institute for Computational Science and Engineering (PICSciE) and Office of Information Technology's Research Computing. B.A.B. and N.R. were supported by the Office of Naval Research (ONR Grant No. N00014-20-1-2303), U.S. Department of Energy (Grant No. DE-SC0016239), and were partially supported by the National Science Foundation (EAGER Grant No. DMR 1643312), a Simons Investigator grant (No. 404513), the Packard Foundation, the Schmidt Fund for Innovative Research, the BSF Israel US foundation (Grant No. 2018226), the Gordon and Betty Moore Foundation through Grant No. GBMF8685 towards the Princeton theory program, and a Guggenheim Fellowship from the John Simon Guggenheim Memorial Foundation. B.A.B. and N.R. were also supported by the NSF-MRSEC (Grant No. DMR-2011750). B.A.B. and N.R. gratefully acknowledge financial support from the Schmidt DataX Fund at Princeton University made possible through a major gift from the Schmidt Futures Foundation. This work is also partly supported by a project that has received funding from the European Research Council (ERC) under the European Union's Horizon 2020 research and innovation programme (grant agreement no. 101020833). O. V. is supported by NSF DMR-1916958 and partially by the National High Magnetic Field Laboratory through NSF Grant No. DMR-1157490 and the State of Florida. This work was also supported by the Gordon and Betty Moore Foundation's EPiQS initiative grants GBMF9469 and DOE-BES grant DE-FG02-07ER46419 to A.Y. Other support for the experimental work was provided by NSF-MRSEC through the Princeton Center for Complex Materials NSF-DMR-2011750, NSF-DMR-1904442, ExxonMobil through the Andlinger Center for Energy and the Environment at Princeton, and the Princeton Catalysis Initiative. A.Y. acknowledge the hospitality of the Aspen Center for Physics, which is supported by National Science Foundation grant PHY-1607611, and Trinity College, Cambridge UK where part of this work was carried in with the support of in part by a QuantEmX grant from ICAM and the Gordon and Betty Moore Foundation through Grant GBMF9616.

* bernevig@princeton.edu

[1] R. Bistritzer and A. H. MacDonald, PNAS **108**, 12233 (2011).
[2] J. M. B. Lopes dos Santos, N. M. R. Peres, and A. H. Castro Neto, Phys. Rev. Lett. **99**, 256802 (2007).
[3] E. Suárez Morell, J. D. Correa, P. Vargas, M. Pacheco, and Z. Barticevic, Phys. Rev. B **82**, 121407 (2010).
[4] Y. Cao, V. Fatemi, A. Demir, S. Fang, S. L. Tomarken, J. Y. Luo, J. D. Sanchez-Yamagishi, K. Watanabe, T. Taniguchi, E. Kaxiras, R. C. Ashoori, and P. Jarillo-Herrero, Nature **556**, 80 (2018).
[5] M. Yankowitz, S. Chen, H. Polshyn, Y. Zhang, K. Watanabe, T. Taniguchi, D. Graf, A. F. Young, and C. R. Dean, Science **363**, 1059 (2019).
[6] X. Lu, P. Stepanov, W. Yang, M. Xie, M. A. Aamir, I. Das, C. Urgell, K. Watanabe, T. Taniguchi, G. Zhang, A. Bachtold, A. H. MacDonald, and D. K. Efetov, Nature **574**, 653 (2019).
[7] H. Polshyn, M. Yankowitz, S. Chen, Y. Zhang, K. Watanabe, T. Taniguchi, C. R. Dean, and A. F. Young, Nat. Phys. **15**, 1011 (2019).

[8] Y. Cao, D. Chowdhury, D. Rodan-Legrain, O. Rubies-Bigorda, K. Watanabe, T. Taniguchi, T. Senthil, and P. Jarillo-Herrero, Phys. Rev. Lett. **124**, 076801 (2020).

[9] M. Serlin, C. L. Tschirhart, H. Polshyn, Y. Zhang, J. Zhu, K. Watanabe, T. Taniguchi, L. Balents, and A. F. Young, Science **367**, 900 (2020).

[10] G. Chen, A. L. Sharpe, E. J. Fox, Y.-H. Zhang, S. Wang, L. Jiang, B. Lyu, H. Li, K. Watanabe, T. Taniguchi, Z. Shi, T. Senthil, D. Goldhaber-Gordon, Y. Zhang, and F. Wang, Nature **579**, 56 (2020).

[11] P. Stepanov, I. Das, X. Lu, A. Fahimniya, K. Watanabe, T. Taniguchi, F. H. L. Koppens, J. Lischner, L. Levitov, and D. K. Efetov, Nature **583**, 375 (2020).

[12] X. Liu, Z. Wang, K. Watanabe, T. Taniguchi, O. Vafek, and J. I. A. Li, Science **371**, 1261 (2021).

[13] J. M. Park, Y. Cao, K. Watanabe, T. Taniguchi, and P. Jarillo-Herrero, Nature **592**, 43 (2021).

[14] Y. Saito, J. Ge, K. Watanabe, T. Taniguchi, and A. F. Young, Nat. Phys. **16**, 926 (2020).

[15] S. Wu, Z. Zhang, K. Watanabe, T. Taniguchi, and E. Y. Andrei, Nat. Mater. **20**, 488 (2021).

[16] X. Lu, B. Lian, G. Chaudhary, B. A. Piot, G. Romagnoli, K. Watanabe, T. Taniguchi, M. Poggio, A. H. MacDonald, B. A. Bernevig, and D. K. Efetov, PNAS **118** (2021), 10.1073/pnas.2100006118.

[17] Y. Saito, J. Ge, L. Rademaker, K. Watanabe, T. Taniguchi, D. A. Abanin, and A. F. Young, Nat. Phys. , 1 (2021).

[18] Y. Saito, F. Yang, J. Ge, X. Liu, T. Taniguchi, K. Watanabe, J. I. A. Li, E. Berg, and A. F. Young, Nature **592**, 220 (2021).

[19] Y. Cao, D. Rodan-Legrain, J. M. Park, N. F. Q. Yuan, K. Watanabe, T. Taniguchi, R. M. Fernandes, L. Fu, and P. Jarillo-Herrero, Science **372**, 264 (2021).

[20] A. Kerelsky, L. J. McGilly, D. M. Kennes, L. Xian, M. Yankowitz, S. Chen, K. Watanabe, T. Taniguchi, J. Hone, C. Dean, A. Rubio, and A. N. Pasupathy, Nature **572**, 95 (2019).

[21] Y. Xie, B. Lian, B. Jäck, X. Liu, C.-L. Chiu, K. Watanabe, T. Taniguchi, B. A. Bernevig, and A. Yazdani, Nature **572**, 101 (2019).

[22] Y. Jiang, X. Lai, K. Watanabe, T. Taniguchi, K. Haule, J. Mao, and E. Y. Andrei, Nature **573**, 91 (2019).

[23] Y. Choi, J. Kemmer, Y. Peng, A. Thomson, H. Arora, R. Polski, Y. Zhang, H. Ren, J. Alicea, G. Refael, F. von Oppen, K. Watanabe, T. Taniguchi, and S. Nadj-Perge, Nat. Phys. **15**, 1174 (2019).

[24] D. Wong, K. P. Nuckolls, M. Oh, B. Lian, Y. Xie, S. Jeon, K. Watanabe, T. Taniguchi, B. A. Bernevig, and A. Yazdani, Nature **582**, 198 (2020).

[25] Y. Choi, H. Kim, Y. Peng, A. Thomson, C. Lewandowski, R. Polski, Y. Zhang, H. S. Arora, K. Watanabe, T. Taniguchi, J. Alicea, and S. Nadj-Perge, arXiv:2008.11746 [cond-mat] (2020), arXiv:2008.11746 [cond-mat].

[26] K. P. Nuckolls, M. Oh, D. Wong, B. Lian, K. Watanabe, T. Taniguchi, B. A. Bernevig, and A. Yazdani, Nature **588**, 610 (2020).

[27] Y. Choi, H. Kim, Y. Peng, A. Thomson, C. Lewandowski, R. Polski, Y. Zhang, H. S. Arora, K. Watanabe, T. Taniguchi, J. Alicea, and S. Nadj-Perge, Nature **589**, 536 (2021).

[28] Y. Choi, H. Kim, C. Lewandowski, Y. Peng, A. Thomson, R. Polski, Y. Zhang, K. Watanabe, T. Taniguchi, J. Alicea, and S. Nadj-Perge, Nat. Phys. **17**, 1375 (2021).

[29] C. L. Tschirhart, M. Serlin, H. Polshyn, A. Shragai, Z. Xia, J. Zhu, Y. Zhang, K. Watanabe, T. Taniguchi, M. E. Huber, and A. F. Young, Science **372**, 1323 (2021).

[30] N. F. Q. Yuan and L. Fu, Phys. Rev. B **98**, 045103 (2018).

[31] M. Ochi, M. Koshino, and K. Kuroki, Phys. Rev. B **98**, 081102 (2018).

[32] A. Thomson, S. Chatterjee, S. Sachdev, and M. S. Scheurer, Phys. Rev. B **98**, 075109 (2018).

[33] J. F. Dodaro, S. A. Kivelson, Y. Schattner, X. Q. Sun, and C. Wang, Phys. Rev. B **98**, 075154 (2018).

[34] X. Y. Xu, K. T. Law, and P. A. Lee, Phys. Rev. B **98**, 121406 (2018).

[35] M. Koshino, N. F. Q. Yuan, T. Koretsune, M. Ochi, K. Kuroki, and L. Fu, Phys. Rev. X **8**, 031087 (2018).

[36] H. C. Po, L. Zou, A. Vishwanath, and T. Senthil, Phys. Rev. X **8**, 031089 (2018).

[37] J. W. F. Venderbos and R. M. Fernandes, Phys. Rev. B **98**, 245103 (2018).

[38] D. M. Kennes, J. Lischner, and C. Karrasch, Phys. Rev. B **98**, 241407 (2018).

[39] T. Huang, L. Zhang, and T. Ma, Science Bulletin **64**, 310 (2019).

[40] J. Liu, J. Liu, and X. Dai, Phys. Rev. B **99**, 155415 (2019).

[41] X.-C. Wu, C.-M. Jian, and C. Xu, Phys. Rev. B **99**, 161405 (2019).

[42] L. Classen, C. Honerkamp, and M. M. Scherer, Phys. Rev. B **99**, 195120 (2019).

[43] J. Kang and O. Vafek, Phys. Rev. Lett. **122**, 246401 (2019).

[44] K. Seo, V. N. Kotov, and B. Uchoa, Phys. Rev. Lett. **122**, 246402 (2019).

[45] Y. Da Liao, Z. Y. Meng, and X. Y. Xu, Phys. Rev. Lett. **123**, 157601 (2019).

[46] F. Wu and S. Das Sarma, Phys. Rev. Lett. **124**, 046403 (2020).

[47] M. Xie and A. H. MacDonald, Phys. Rev. Lett. **124**, 097601 (2020).

[48] N. Bultinck, S. Chatterjee, and M. P. Zaletel, Phys. Rev. Lett. **124**, 166601 (2020).

[49] A. Davydov, K. Choo, M. H. Fischer, and T. Neupert, Phys. Rev. B **105**, 165153 (2022).

[50] D. V. Chichinadze, L. Classen, and A. V. Chubukov, Phys. Rev. B **102**, 125120 (2020).

[51] S. Chatterjee, N. Bultinck, and M. P. Zaletel, Phys. Rev. B **101**, 165141 (2020).

[52] C. Repellin, Z. Dong, Y.-H. Zhang, and T. Senthil, Phys. Rev. Lett. **124**, 187601 (2020).

[53] K. Hejazi, X. Chen, and L. Balents, Phys. Rev. Research **3**, 013242 (2021).

[54] T. Cea and F. Guinea, Phys. Rev. B **102**, 045107 (2020).

[55] Y. Zhang, K. Jiang, Z. Wang, and F. Zhang, Phys. Rev. B **102**, 035136 (2020).

[56] J. Kang and O. Vafek, Phys. Rev. B **102**, 035161 (2020).

[57] R. M. Fernandes and J. W. F. Venderbos, Science Advances **6**, eaba8834 (2020).

[58] E. Brillaux, D. Carpentier, A. A. Fedorenko, and L. Savary, arXiv:2008.05041 [cond-mat] (2020), arXiv:2008.05041 [cond-mat].

[59] N. Bultinck, E. Khalaf, S. Liu, S. Chatterjee, A. Vish-

wanath, and M. P. Zaletel, Phys. Rev. X **10**, 031034 (2020).
[60] M. Xie and A. H. MacDonald, Phys. Rev. Lett. **127**, 196401 (2021).
[61] T. Soejima, D. E. Parker, N. Bultinck, J. Hauschild, and M. P. Zaletel, Phys. Rev. B **102**, 205111 (2020).
[62] M. Christos, S. Sachdev, and M. S. Scheurer, PNAS **117**, 29543 (2020).
[63] P. Eugenio and C. Dag, SciPost Physics Core **3**, 015 (2020).
[64] O. Vafek and J. Kang, Phys. Rev. Lett. **125**, 257602 (2020).
[65] S. Liu, E. Khalaf, J. Y. Lee, and A. Vishwanath, Phys. Rev. Research **3**, 013033 (2021).
[66] Y. Da Liao, J. Kang, C. N. Breiø, X. Y. Xu, H.-Q. Wu, B. M. Andersen, R. M. Fernandes, and Z. Y. Meng, Phys. Rev. X **11**, 011014 (2021).
[67] J. Liu and X. Dai, Phys. Rev. B **103**, 035427 (2021).
[68] J. Kang, B. A. Bernevig, and O. Vafek, Phys. Rev. Lett. **127**, 266402 (2021).
[69] B. Lian, Z.-D. Song, N. Regnault, D. K. Efetov, A. Yazdani, and B. A. Bernevig, Phys. Rev. B **103**, 205414 (2021).
[70] F. Xie, A. Cowsik, Z.-D. Song, B. Lian, B. A. Bernevig, and N. Regnault, Phys. Rev. B **103**, 205416 (2021).
[71] D. E. Parker, T. Soejima, J. Hauschild, M. P. Zaletel, and N. Bultinck, Phys. Rev. Lett. **127**, 027601 (2021).
[72] Y. H. Kwan, G. Wagner, T. Soejima, M. P. Zaletel, S. H. Simon, S. A. Parameswaran, and N. Bultinck, Phys. Rev. X **11**, 041063 (2021).
[73] B.-B. Chen, Y. D. Liao, Z. Chen, O. Vafek, J. Kang, W. Li, and Z. Y. Meng, Nat Commun **12**, 5480 (2021).
[74] G. Wagner, Y. H. Kwan, N. Bultinck, S. H. Simon, and S. A. Parameswaran, Phys. Rev. Lett. **128**, 156401 (2022).
[75] B. A. Bernevig, Z.-D. Song, N. Regnault, and B. Lian, Phys. Rev. B **103**, 205413 (2021).
[76] B. A. Bernevig, B. Lian, A. Cowsik, F. Xie, N. Regnault, and Z.-D. Song, Phys. Rev. B **103**, 205415 (2021).
[77] P. Coleman, *Introduction to Many-Body Physics* (Cambridge University Press, Cambridge, 2015).
[78] X. Liu, G. Farahi, C.-L. Chiu, Z. Papic, K. Watanabe, T. Taniguchi, M. P. Zaletel, and A. Yazdani, Science **375**, 321 (2022).
[79] A. Coissard, D. Wander, H. Vignaud, A. G. Grushin, C. Repellin, K. Watanabe, T. Taniguchi, F. Gay, C. B. Winkelmann, H. Courtois, H. Sellier, and B. Sacépé, Nature **605**, 51 (2022).
[80] X. Li, F. Wu, and A. H. MacDonald, arXiv:1907.12338 [cond-mat] (2019), arXiv:1907.12338 [cond-mat].
[81] I. Das, X. Lu, J. Herzog-Arbeitman, Z.-D. Song, K. Watanabe, T. Taniguchi, B. A. Bernevig, and D. K. Efetov, Nat. Phys. **17**, 710 (2021).
[82] See Supplemental Material at `http://link.aps.org/supplemental/xxx` for details about the single-particle and interaction TBG Hamiltonians, the spectral function, the charge one-excitation spectra and the parameterizations of the spectral function matrix elements, which includes Refs. [89–114].
[83] Z. Song, Z. Wang, W. Shi, G. Li, C. Fang, and B. A. Bernevig, Phys. Rev. Lett. **123**, 036401 (2019).
[84] J. Kang and O. Vafek, Phys. Rev. X **8**, 031088 (2018).
[85] Z.-D. Song, B. Lian, N. Regnault, and B. A. Bernevig, Phys. Rev. B **103**, 205412 (2021).
[86] H. C. Po, L. Zou, T. Senthil, and A. Vishwanath, Phys. Rev. B **99**, 195455 (2019).
[87] G. Tarnopolsky, A. J. Kruchkov, and A. Vishwanath, Phys. Rev. Lett. **122**, 106405 (2019).
[88] J. P. Hong, T. Soejima, and M. P. Zaletel, arXiv:2110.14674 [cond-mat] (2021), arXiv:2110.14674 [cond-mat].
[89] J. Ahn, S. Park, and B.-J. Yang, Phys. Rev. X **9**, 021013 (2019).
[90] C. R. Ast, B. Jäck, J. Senkpiel, M. Eltschka, M. Etzkorn, J. Ankerhold, and K. Kern, Nat Commun **7**, 13009 (2016).
[91] C. Bao, H. Zhang, T. Zhang, X. Wu, L. Luo, S. Zhou, Q. Li, Y. Hou, W. Yao, L. Liu, P. Yu, J. Li, W. Duan, H. Yao, Y. Wang, and S. Zhou, Phys. Rev. Lett. **126**, 206804 (2021).
[92] A. H. Barnett, J. Magland, and L. af Klinteberg, SIAM J. Sci. Comput. **41**, C479 (2019).
[93] A. H. Barnett, Appl. Comput. Harmon. Anal. **51**, 1 (2021).
[94] B. A. Bernevig, Z.-D. Song, N. Regnault, and B. Lian, Phys. Rev. B **103**, 205411 (2021).
[95] C. Chamon, Phys. Rev. B **62**, 2806 (2000).
[96] S. Dai, Y. Xiang, and D. J. Srolovitz, Nano Lett. **16**, 5923 (2016).
[97] M. M. Ervasti, F. Schulz, P. Liljeroth, and A. Harju, J. Electron Spectrosc. Relat. Phenom. SI: The Electronic Structure of 2D and Layered Materials, **219**, 63 (2017).
[98] V. P. Gusynin, S. G. Sharapov, and J. P. Carbotte, Int. J. Mod. Phys. B **21**, 4611 (2007).
[99] C. Gutiérrez, C.-J. Kim, L. Brown, T. Schiros, D. Nordlund, E. B. Lochocki, K. M. Shen, J. Park, and A. N. Pasupathy, Nat. Phys. **12**, 950 (2016).
[100] I. F. Herbut, V. Juričić, and B. Roy, Phys. Rev. B **79**, 085116 (2009).
[101] M. Ijäs, M. Ervasti, A. Uppstu, P. Liljeroth, J. van der Lit, I. Swart, and A. Harju, Phys. Rev. B **88**, 075429 (2013).
[102] S. K. Jain, V. Juričić, and G. T. Barkema, 2D Mater. **4**, 015018 (2016).
[103] K. Kim, M. Yankowitz, B. Fallahazad, S. Kang, H. C. P. Movva, S. Huang, S. Larentis, C. M. Corbet, T. Taniguchi, K. Watanabe, S. K. Banerjee, B. J. LeRoy, and E. Tutuc, Nano Lett. **16**, 1989 (2016).
[104] M. Koshino, T. Morimoto, and M. Sato, Phys. Rev. B **90**, 115207 (2014).
[105] S.-Y. Li, Y. Zhang, L.-J. Yin, and L. He, Phys. Rev. B **100**, 085437 (2019).
[106] K. Nomura, S. Ryu, and D.-H. Lee, Phys. Rev. Lett. **103**, 216801 (2009).
[107] N. M. R. Peres, L. Yang, and S.-W. Tsai, New J. Phys. **11**, 095007 (2009).
[108] A. A. Radzig and B. M. Smirnov, *Reference Data on Atoms, Molecules, and Ions*, Springer Series in Chemical Physics (Springer-Verlag, Berlin Heidelberg, 1985).
[109] Y. J. Song, A. F. Otte, V. Shvarts, Z. Zhao, Y. Kuk, S. R. Blankenship, A. Band, F. M. Hess, and J. A. Stroscio, Review of Scientific Instruments **81**, 121101 (2010).
[110] K. Uchida, S. Furuya, J.-I. Iwata, and A. Oshiyama, Phys. Rev. B **90**, 155451 (2014).
[111] J. Wang, Y. Zheng, A. J. Millis, and J. Cano, Phys. Rev. Research **3**, 023155 (2021).
[112] M. M. van Wijk, A. Schuring, M. I. Katsnelson, and

A. Fasolino, 2D Mater. **2**, 034010 (2015).
[113] D. Wong, S. Jeon, K. P. Nuckolls, M. Oh, S. C. J. Kingsley, and A. Yazdani, Review of Scientific Instruments **91**, 023703 (2020).
[114] J. R. Yates, X. Wang, D. Vanderbilt, and I. Souza, Phys. Rev. B **75**, 195121 (2007).